G. B. Hotchkiss
Texas Instruments Incorporated,
Dallas, Texas

L. C. Burmeister
Mechanical Engineering Department.

K. A. Bishop
Chemical and Petroleum
Engineering Department.

The University of Kansas,
Lawrence, Kansas 66045

Solar Collector Parameter Identification From Unsteady Data by a Discrete-Gradient Algorithm

A discrete-gradient algorithm is used to identify the parameters in a one-node and a two-node capacitance model of a flat-plate collector. Collector parameters are first obtained by a linear-least-squares fit to steady state data. These parameters, together with the collector heat capacitances, are then separately determined from unsteady data by use of the discrete-gradient algorithm with less than 10 percent deviation from the steady-state determination. All data were obtained in the indoor solar simulator at the NASA Lewis Research Center.

Introduction

Much of the testing of flat-plate collectors must be done out-of-doors by exposure to the sun [1]. But because collector parameters depend on such variables as wind speed, temperature, and incidence angle, which are uncontrollable out-of-doors, the performance data there are often greatly scattered [2]. Part of this scatter is also attributable to the unsteady character of the insolation (except, perhaps, at solar noon on a clear day) and the application of steady state relations to such unsteady situations [3].

One alternative to outdoor testing is to use an indoor solar simulator which duplicates many of the sun's characteristics as they appear to a solar collector on Earth. Such a solar simulator was constructed and evaluated by Simon and Harlamert [4] and Simon [5–9]. Control of environmental conditions, including the simulated insolation, allows acquisition of very consistent and accurate steady data whose reduction is simple.

However, the inability of an indoor solar simulator to accurately account for regional variations of outdoor conditions leaves outdoor testing of flat-plate collectors still a desirable procedure. Additionally, outdoor testing would be convenient for detecting a possible change of an installed flat-plate collector's parameters after a period of service.

If accurate outdoor testing is to be done rapidly, the heat capacitance of the flat-plate collector must be taken into account since outdoor conditions are rarely steady for long. A common mathematical model of a flat-plate collector, often referred to as the Hottell-Whillier-Bliss [10, 11] model, is an algebraic equation and presumes that steady conditions prevail. Mathematical models of flat-plate collectors in unsteady conditions include heat capacitance effects, such as were considered by Klein, Duffie, and Beckman [12], and are differential equations. The heat capacitances of the absorber plate, covers, base, and fluid are influential in the unsteady state.

This paper describes a testing procedure that trades the simplicity of a steady state data reduction procedure for the simplicity of uncontrolled unsteady state test conditions, thereby making it applicable to collectors which have been installed as well as to prototype designs. In this study, a discrete-gradient algorithm is applied to the task of identifying the parameters in the differential equations for one-node and two-node capacitance models of a flat-plate collector in unsteady conditions. This is accomplished by minimization of an integral (over time)-squared-error criterion which compares measured coolant outlet temperature with that predicted by the model. The utility of that testing procedure is demonstrated by treatment of data for a specific set of conditions with a specific algorithm rather than exhaustively testing the performance of a variety of algorithms with data for a wide range of conditions.

Mathematical Models of Flat-Plate Collectors

Derivation of mathematical models of flat-plate collectors begins by applying the conservation of energy principle to the collector or to a part of the collector. This principle requires that

rate of energy storage in collector part +

rate of energy convection from part by coolant $= q_{\text{net}}$ (1)

where q_{net} is the net rate at which energy is collected by the collector part.

Steady-State Model. Viewing the collector as a whole, the net rate at which energy is collected by a flat-plate collector is given for the steady state [13, 14] as

$$q_{\text{net}} = A\acute{F}[(\tau\alpha)I - U_L(\bar{T}_f - T_a)] \tag{2}$$

from which the collector efficiency η follows as

$$\eta = q_{\text{net}}/IA = \acute{F}(\tau\alpha) - \acute{F}U_L(\bar{T}_f - T_a)/I \tag{3}$$

Equation (2) relates the heat loss from the collector to the average coolant fluid temperature $\bar{T}_f$ and uses a plate efficiency factor $\acute{F}$. If collector efficiency is plotted versus the ratio of temperature difference to insolation, $(\bar{T}_f - T_a)/I$, equation (3) shows that a straight line will result if the

Contributed by the Solar Energy Division for publication in the JOURNAL OF SOLAR ENGINEERING. Manuscript received by the Solar Energy Division, March, 1982.

parameters $\acute{F}(\tau\alpha)$ and $\acute{F}U_L$ are constant. The intercept on the ordinate of such a plot gives $\acute{F}(\tau\alpha)$ and the slope gives $\acute{F}U_L$.

The plate efficiency factor $\acute{F}$ is used in this study because the heat loss from the collector depends on both the inlet and outlet temperature of the coolant. In the unsteady state considered in a later part of this study, the outlet temperature varies while the inlet temperature is held constant. The commonly used heat removal factor F_R relates heat loss from the collector only to the inlet temperature. While both $\acute{F}$ and F_R are based on steady-state ideas, $\acute{F}$ is believed to be more appropriate for the unsteady conditions to be considered later.

The $\acute{F}$ factor is very nearly constant [11], but $(\tau\alpha)$ is noticeably dependent on incidence angle, and U_L is noticably dependent on temperature level and wind speed [14]. The indoor solar simulator measurements of Simon [7, 8] confirm these observations. Nevertheless, $\acute{F}(\tau\alpha)$ and $\acute{F}U_L$ can be taken to be constant if either some uncertainly is allowable or if only a narrow range of operating conditions is faced.

One-Node Model. In the unsteady state some of the net energy collected is stored in the collector, the remainder being convected away by the coolant. Again viewing the collector as a whole, one has

$$\text{rate of energy storage in collector} = A\ C_c d\bar{T}_f/dt \tag{4}$$

if a one-node capacitance model is adopted as was done by Close [15]. This presumes that the total energy stored in the collector is proportional to the change of a single temperature, here taken to be the average coolant fluid temperature $\bar{T}_f$. The effect of the coolant is given by

$$\text{rate of energy convection from collector by coolant} = A\ G\ C_p(T_o - T_i) \tag{5}$$

which is, of course, also applicable to a steady state view of the entire collector. Inserting equations (2), (4), and (5) into equation (1) and employing the approximation that the average fluid temperature is the arithmetic average of the fluid's inlet and outlet temperatures, $\bar{T}_f = (T_o + T_i)/2$, gives the one-node model as

$$C_c dT_0/dt = 2\acute{F}(\tau\alpha)I - \acute{F}U_L(T_0 + T_i - 2T_a) - 2\ G\ C_p(T_0 - T_i) + C_c dT_i/dt \tag{6}$$

Two-Node Model. The one-node model of equation (6) possesses the virtue of simplicity, being a first-order differential equation. However, it does not account for the fact that the glazing (which represent an appreciable part of the collector's heat capacitance) would experience a different temperature change from that of the absorber plate-coolant combination. To account for this, energy balances are separately made on the glazing (assumed to be a single glazing) and on the absorber plate-coolant combination.

An energy balance on the glazing leads to

$$C_g dT_g/dt = (\bar{T}_f - T_g)/R_1 - (T_g - T_a)/R_2 \tag{7}$$

in which T_g is the glazing temperature, C_g is the glazing heat capacitance, R_1 is the resistance to heat flow from the absorber to the glazing, and R_2 is the resistance to heat flow from the glazing to the ambient air. Equation (7) does not account for the direct energy gained by the glazing due to absorption of insolation, a simplification that is believed to be appropriate for a preliminary study. The assumption of constant R_1 and R_2 is believed to be of satisfactory accuracy since the outlet temperature to be considered fluctuates roughly 3 C (5 F) about a mean value as shown in Fig. 4. An energy balance on the absorber plate-coolant combination in the manner described in the derivation of equation (6) leads to

$$C_c d\bar{T}_f/dt = \acute{F}(\tau\alpha)I - (\bar{T}_f - T_g)/R_1 - G\ C_p(T_0 - T_i) \tag{8}$$

Solving for T_g from equation (8), inserting that result into equation (7), recognizing that $1/(R_1 + R_2) = \acute{F}U_L$ and again employing the approximation that the average fluid temperature is the arithmetic mean of the fluid's inlet and outlet temperatures, $\bar{T}_f = (T_0 + T_i)/2$, gives the two-node mathematical model of a flat-plate collector as

$$\begin{aligned} b_4 d^2T_0/dt^2 + b_3 dT_0/dt &= 2\acute{F}(\tau\alpha)I \\ &\quad - \acute{F}U_L(T_0 + T_i - 2T_a) - 2G\ C_p(T_0 - T_i) \\ &\quad + \{b_5[\acute{F}(\tau\alpha)dI/dt - C_p(T_0 - T_i)dG/dt] \\ &\quad + (2G\ C_p b_5 - b_3)dT_i/dt - b_4 d^2T_i/dt^2\} \end{aligned} \tag{9}$$

Nomenclature

A = area, m^2
$\bar{B}$ = column vector of model parameters
$B_{1,2,3,4}$ = defined in equation (10) or (11)
$b_{3,4,5}$ = defined in equation (9)
C_c = collector heat capacitance, kJ/m^2-C
C_g = glazing heat capacitance, kJ/m^2-C
C_{c_c} = collector heat capacity for "cool-down," kJ/m^2-C
C_{c_w} = collector heat capacity for "warm-up," kJ/m^2-C
C_p = specific heat of collector fluid, kJ/kg-C
e = difference between mathematical model output and process output, $e = y - T_0$, C
exp = base of natural or Napierian logarithm, = 2.718 . . .
$\acute{F}$ = collector plate efficiency factor, dimensionless
f = objective function, $f = 1/2 \int_{t_i}^{t_i + \Delta t} e^2 dt$
G = coolant flow rate per unit area, kg/hr-m^2
I = solar radiation incident upon the collector, W/m^2
K_n = gain of the optimization algorithm for the nth parameter
q = heat flow rate, W
R_1 = absorber-glazing thermal resistance, m^2-C/W
R_2 = glazing-air thermal resistance, m^2-C/W
T_a = ambient air temperature, C
$\bar{T}_f$ = average collector fluid temperature, C
T_g = glazing temperature, C
T_i = coolant inlet temperature, C
T_0 = coolant outlet temperature, C
t = time, hr
t_i = time at the beginning of an optimization iteration, hr
Δt = time interval for gradient computation or for data smoothing, hr
U_L = overall collector heat loss coefficient, W/m^2-C
u_n = sensitivity coefficient, $u_n = \partial F/\partial B_n$
y = mathematical model output
$(\tau\alpha)$ = effective absorptance-transmittance product, dimensionless
η = collector efficiency, dimensionless
τ = time constant, hr
τ_c = collector time constant for "cool-down," hr
τ_w = collector time constant for "warm-up," hr

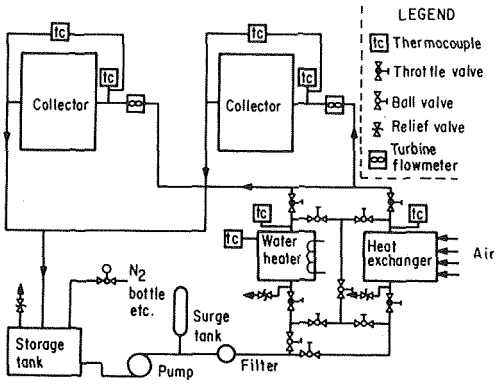

Fig. 1 Schematic of the liquid flow loop

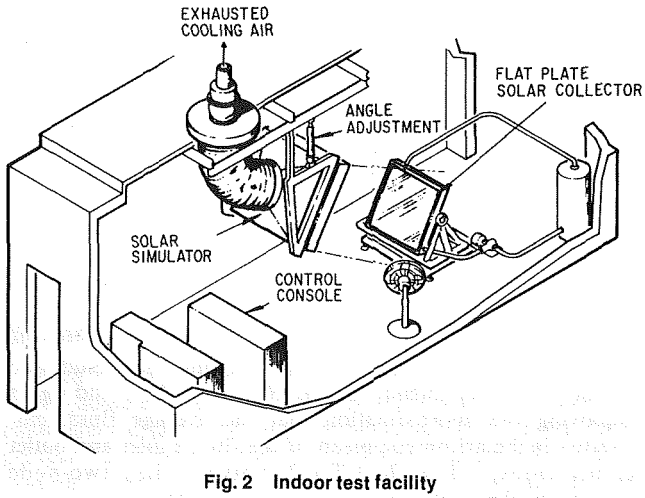

Fig. 2 Indoor test facility

where

$$b_3 = C_c + C_g(1 + 2R_1 G\, C_p)(1 - R_1 \acute{F} U_L),$$

$$b_4 = R_1 C_g C_c (1 - R_1 \acute{F} U_L),$$

and

$$b_5 = 2R_1 C_g (1 - R_1 \acute{F} U_L).$$

The two-node mathematical model of equation (9) is more complex than the one-node model of equation (6), being a second-order differential equation. Multiple glazings could be taken into account, if that would substantially improve the descriptive ability of a mathematical model, at the sacrifice of increasing the order of the final describing differential equation by one for each glazing.

Neither the one-node nor the two-node models consider the effects of the residence time of a fluid particle in the collector.

Experimentation

The test apparatus is shown schematically in Fig. 1. The heat exchanger and immersion heater indicated in Fig. 1 allowed the collector inlet temperature to be held constant. The indoor solar simulator in which the experimentation was done is illustrated in Fig. 2 and consisted of 143 tungsten halogen 300 watt lamps whose output was collimated by Fresnel lenses.

The collector inlet and outlet temperatures, T_i and T_0, were measured with ISA type T (copper-constantan) thermocouples calibrated at 0 C (32 F) and 100 C (212 F). The error in absolute temperature measurement was less than 0.44 C (0.8 F) and the differential temperature error between the inlet and outlet thermocouples was less than 0.22 C (0.4 F). The temperature difference, $T_0 - T_i$, of the fluid across the solar collectors was also measured with a thermopile which had 10 ISA type E (chromel-constantan) thermocouples connected in series.

The coolant flowrate of the 50/50 by weight mixture of water and ethylene-glycol was determined within 2 percent of the indicated flow with a calibrated turbine-type flow meter.

The ambient temperature was measured with an ISA type T thermocouple mounted in a radiation shield. The simulated solar flux was normal to the collector and was measured with a water-cooled Gardon type radiometer (calibrated with a National Bureau of Standards standard source of irradiance) oriented at the collector tilt angle.

The millivolt-level electrical outputs of the measuring instruments were recorded on a data logger. Later, the data were transferred to cards for data reduction on a digital computer.

The collector tested was manufactured by Honeywell, Inc. (under NASA Contract No. NAS3-17862) of Minneapolis, Minn. It has a steel spot-welded absorber plate whose area is 1.24 m^2 (13.3 ft^2), a selective coating of black chrome, two glazing of glass, and an aluminum collector housing. Overall dimensions are 1.22 × 1.22 × 0.15 m (4 × 4 × 0.5 ft).

The steady-state test procedures used were based on the ASHRAE testing standards [16]. In the indoor simulator a fan simulated wind at 3.13 m/sec (7 mph) steadily blowing across the collector. Before the solar simulator was turned on, the collector was given time (approximately 1 hr) to achieve thermal equilibrium at the chosen inlet temperature. After the solar simulator was turned on, transient "warm-up" data were recorded every 4 sec. Data were also recorded in the steady-state conditions which occurred in 10–15 min. The simulator lamps were then turned off and transient "cool-down" data were recorded every 4 seconds.

The unsteady-state test procedures included simulation of a square-wave variation of insolation. This was accomplished by intermittently placing a sheet of cardboard between the collector and the solar simulator's lamps, with coolant flow rate and inlet temperature held constant and with the solar simulator itself operating at steady conditions. The collector was allowed to first achieve steady operating conditions at the solar simulator's selected level of insolation. Then the cardboard sheet was quickly introduced, effectively blocking the insolation, and was left in place for several time constants of the collector. It was then quickly removed, allowing the simulated insolation to strike the collector for several time constants of the collector. This procedure was repeated for three or four cycles.

A total of seven variables were recorded, and the most rapid scan rate of the data logger was 4 sec. Thus, each variable was recorded once each 4 sec. and the instants at which different variables were recorded did not coincide exactly.

Greater detail of equipment and procedure is given by Hotchkiss [17]. He gives more extensive measurements made on the NASA/Honeywell collector than those used in this study as well as measurements made on a different collector.

Results

Data, taken as described in the preceding section, were analyzed using three different procedures. Steady-state data were used to develop steady-state efficiency curves from which the parameters $\acute{F}U_L$ and $\acute{F}(\tau\alpha)$ can be determined. Transient heat-up and cool-down data were used to determine heat-up and cool-down time constants (assuming a one-node model for the collector). Finally, transient data were used in conjunction with the discrete-gradient procedure to identify the parameters specified for the one-node and two-node models.

Steady-State Model Results. Steady-state efficiency

Table 1 Performance constants of the NASA/Honeywell collector from steady-state data

G,kg/hr-m^2	$\acute{F}(\tau\alpha)$, dimensionless	$\acute{F}U_L$, W/m^2-C
48.8	0.815	4.583
97.6	0.845	4.662

Table 2 Collector time constants for "warm-up," τ_w, and "cool-down," τ_c, of the NASA/Honeywell collector with $G = 48.8$ kg/hr-m^2 (10 lbm/hr-ft^2)

T_i,C	τ_w,hr	τ_c,hr
Ambient	0.0522 (188 sec)	0.0544 (196 sec)
48.9	0.0489 (176 sec)	0.0544 (196 sec)
71.1	0.0578 (208 sec)	0.0578 (208 sec)
87.8	0.0578 (208 sec)	0.0656 (236 sec)

Table 3 Collector heat capacitance for "warm-up, C_{c_w}, and "cool-down," C_{c_c}, of the NASA/Honeywell collector with $G = 48.8$ kg/hr-m^2 (10 lbm/hr-ft^2)

Ambient	18.419	19.339
48.9	17.560	19.666
71.1	21.424	21.547
87.8	21.628	24.552

curves determined by a least-squares fit to the steady-state data for the NASA/Honeywell collector at two different fluid flow rates are shown in Fig. 3. The average fluid temperature, $\bar{T}_f$, in Fig. 3 is defined to be the arithmetic average of the fluid inlet and outlet temperatures. The parameters $\acute{F}U_L$ and $\acute{F}(\tau\alpha)$ were obtained from the slope and intercept of the correlating lines and appear in Table 1. The data of Fig. 3 suggests a slight curvature which is consistent with the arguments of Simon and Buyco [18] regarding the slight temperature dependence of U_L.

Transient Cool-Down and Warm-Up Results. A collector's heat capacitance gives rise to a time constant τ which the one-node mathematical model of equation (6) shows to be related to the other collector parameters by

$$\tau = C_c/[\acute{F}U_L + 2\ G\ C_p]$$

The GC_p parameter was known by direct measurement and the $\acute{F}U_L$ parameter was determined from the steady-state efficiency curve as explained in the foregoing.

The time constant of a collector is defined as the time required for the coolant's outlet temperature to attain 63.2 percent, $1 - \exp(-1)$, of its ultimate change following a step change in insolation. The time constants for a transient "warm-up" τ_w and a transient "cool-down" τ_c accordingly determined for the NASA/Honeywell collector at different coolant inlet temperatures are shown in Table 2 for a coolant flow rate of 48.8 kg/hr-m^2 (10 lbm/hr-ft^2).

Determination of the collector time constant τ then allows the collector's heat capacitance C_c to be evaluated. The collector heat capacitances C_c associated with these time constants are given in Table 3.

Examination of Tables 2 and 3 reveals that the time constants and heat capacitances for collector "warm-up" are consistently less than for "cool-down". Although the differences are fairly small, of the order of 10 percent, they do suggest that a one-node mathematical model for the collector is not able to accurately represent all of the collector's transient characteristics.

For these reasons, the results given in Table 3 should only be regarded as reasonable estimates of the collector's effective heat capacitance. A more refined mathematical model would be expected to give slightly different numerical values of this parameter.

Discrete-Gradient Results. The flat-plate collector is better represented with the two-node model of equation (9).

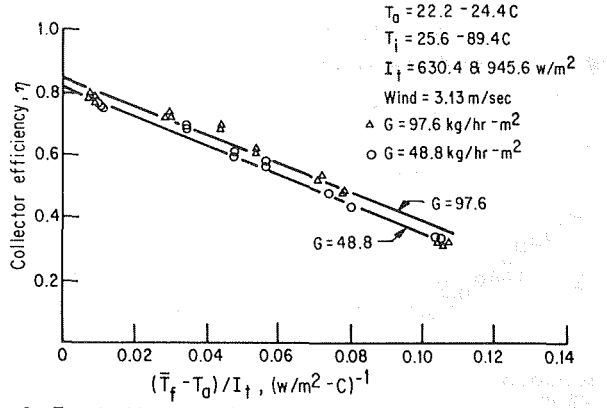

Fig. 3 Zero-incidence performance curve of the NASA/Honeywell collector

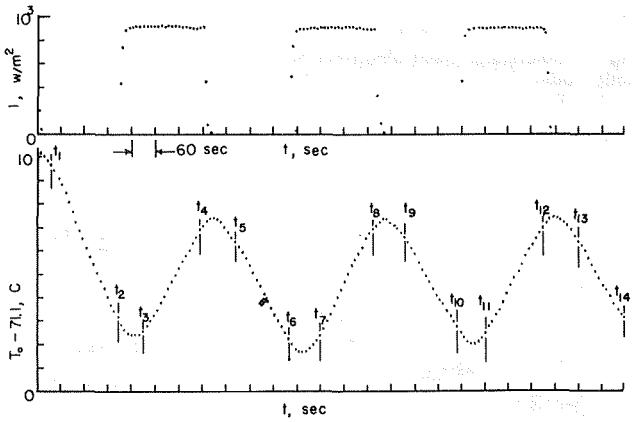

Fig. 4 Simulated insolation and coolant outlet temperature data versus time

For the data treated here, the coolant flow rate and inlet temperature were held very nearly constant and the insolation was either present nearly as a constant or was absent entirely, varying as a square wave due to intermittent interruption by a sheet of cardboard. With these simplifications the two-node mathematical model of the collector of equation (9) reduces to

$$d^2y/dt^2 + (B_3/B_4)dy/dt = [2B_1 I - B_2(y + T_i - 2T_a) - 2GC_p(y - T_i)]/B_4 \qquad (10)$$

Here, y is the coolant outlet temperature predicted by equation (10) with $B_{1,2,3,4}$ being estimated values of $\acute{F}(\tau\alpha)$, $\acute{F}U_L$, b_3, and b_4, respectively.

The parameters of B_1, B_2, B_3, and B_4 were adjusted from their initially estimated values by a discrete-gradient algorithm which minimized an integral (over a brief time) of an error squared. This error was the difference between the time-dependent coolant outlet temperatures predicted by equations (10), y, and measured, T_0. The discrete-gradient algorithm which was implemented on a digital computer is described in the Appendix, where equations (A-3) and (A-5) can be consulted for details pertinent to a two-node model. Minimization of this objective function by repeated adjustment of the four parameters gives a final value of B_1 which is the estimate of $\acute{F}(\tau\alpha)$ and a final value of B_2 which is the estimate of $\acute{F}U_L$. The final values of B_3 and B_4 are the estimates of b_3 and b_4 which are closely associated with the heat capacitances of the collector parts as the derivation of equation (9) suggests although the heat capacitances cannot be directly determined from this information for the conditions of this study.

The data treated by the discrete-gradient algorithm are displayed in Fig. 4 which shows every other pair of insolation

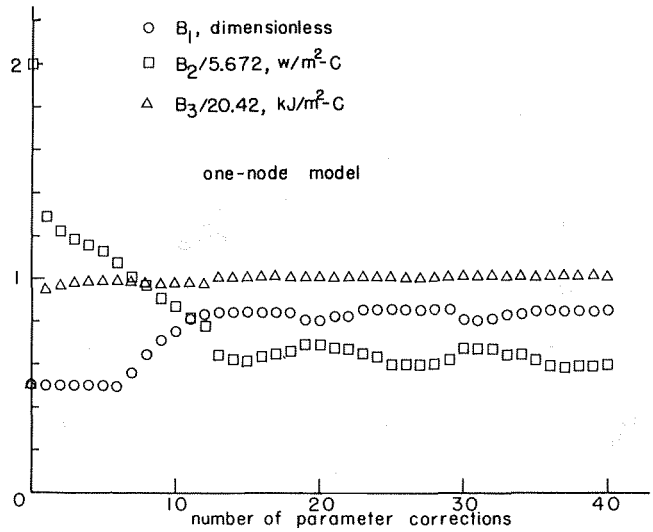

Fig. 5 Discrete-gradient algorithm behavior versus time for the one-node model

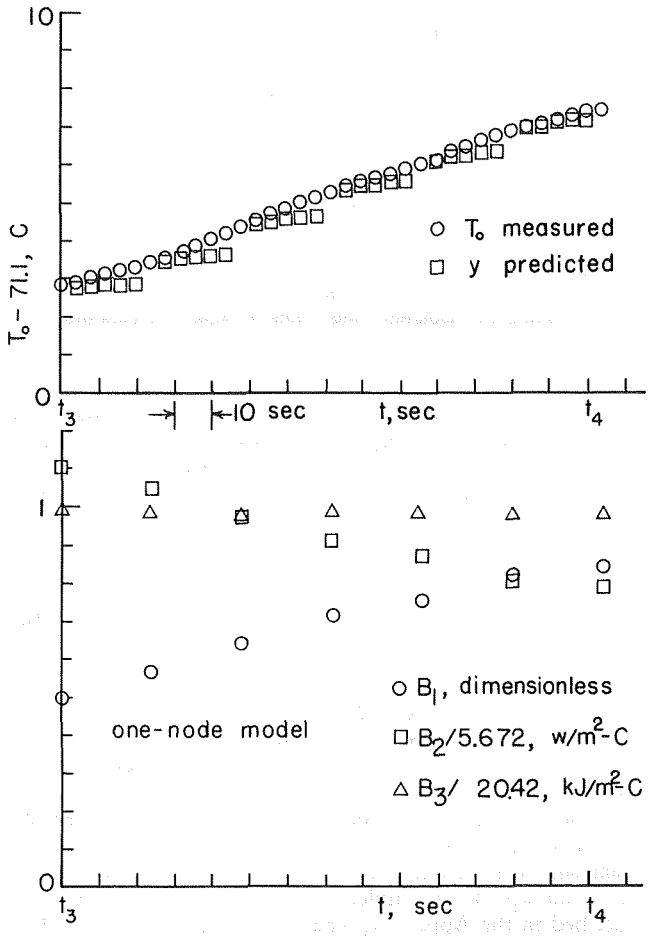

Fig. 6 One-node model parameters versus number of parameter corrections

and outlet temperature measurements made at 4 sec. intervals. The simulated insolation actually varied as a square wave, the radiometer's slow transient response accounting for the rounding of the leading and trailing edges. The coolant outlet temperature shown in Fig. 4 has been smoothed, to reduce the effects of noise and of finite measurement resolution, according to

$$T_{0_{\text{smooth}}}(t) = [T_0(t+\Delta t) + 2\,T_0(t) + T_0(t-\Delta t)]/4$$

with $\Delta t = 4$ sec. From this smoothed data, the value of dT_0/dt required by the discrete-gradient algorithm was estimated by central differences as

$$dT_0(t)/dt = [T_{0_{\text{smooth}}}(t+\Delta t) - T_{0_{\text{smooth}}}(t-\Delta t)]/2\Delta t$$

with $\Delta t = 4$ sec. Preliminary computations showed that such smoothing, or filtering, of data increases the accuracy of parameter identification. In general it has been empirically determined [19] that identification usually underestimates actual values whenever noise exists in data.

The two-node matematical model used, equation (10), does not account for the effects of a fluid particle's residence time in the collector. To reduce error due to this inadequacy of the model, the discrete-gradient algorithm was rendered inoperative for a period of about 90 sec. just after the simulated insolation was either interrupted or resumed. The data used was that in the time intevals of $t_1 - t_2$, $t_3 - t_4$, $t_5 - t_6$, $t_7 - t_8$, $t_9 - t_{10}$, $t_{11} - t_{12}$, and $t_{13} - t_{14}$. Although not shown in Fig. 4, the instantaneous measured coolant inlet temperatures and flow rates were used in the computations even though they were nearly constant. The complete data is available elsewhere [17].

In the digital computer program which implemented the discrete-gradient algorithm, the objective function (the integral over time of the square of the deviation between predicted and measured outlet temperatures) was evaluated for a time interval of 24 sec. Various values of this time interval were tried, ranging from 16–30 sec with no apparent effect.

Various values of the optimizer gains were tried, producing a significant effect. Very small gains, although reducing sensitivity to measurement errors, require many steps to reach convergence since very small parameter adjustments are then made at any one step of the procedure. On the other hand, very large gains can make the procedure unstable [21]. Selection of appropriate gains rapidly increases in difficulty with an increase in the number of parameters being identified.

The procedure employed in this study was to employ the one-node model to achieve preliminary identification of $B_{1,2,3}$. Following this, a more refined parameter identification was achieved by employing the two-node model of equation (10).

The one-node model of equation (6) reduces to

$$dy/dt = [2B_1 T - B_2(y + T_i - 2T_a) - 2GC_p(y - T_i)]/B_3 \qquad (11)$$

Here, B_1 and B_2 represent estimates of $F(\tau\alpha)$ and FU_L while B_3 represents the estimate of C_c in equation (6). Hence, the heat capacitance of a one-node model can be directly determined for the conditions of this study. Equations (*A*-6) and (*A*-8) of the Appendix can be consulted for additional details of the discrete-gradient algorithm applied to the one-node model.

Figures 4–6 illustrate the results of applying the algorithm with Fig. 5 showing details of the application between times t_3 and t_4 which are indicated in Fig. 4. Figure 5 shows that parameter corrections, made after accumulating the error between predicted and measured outlet temperatures, improve the one-mode model's predictive ability and fairly quickly improve the initial estimates of the three parameters. The three parameters' values versus the number of parameter changes are shown in Fig. 6 for the full data shown in Fig. 4. In Fig. 6 it is seen that parameter estimates initially in error by a factor of two are identified within the limitations of the one-node model after about 20 corrections. The gains used were $K_1 = -10\text{F}^{-2} - \text{sec}^{-1}$, $K_2 = -30$ Btu/hr²-ft⁴-F⁴-sec, and $K_3 = -10$ Btu/ft⁴-F⁴-sec; gains within a factor of three of these were also found by trial and error to give statisfactory performance.

The B_3 parameter is soon identified to be nearly a constant. The B_2 parameter exhibits substantial oscillation, being low

during a cooling phase (when insolation is absent, as evidenced by an unchanging value of B_3) and high during a warming phase (when insolation is present nearly as a constant), a difference primarily attributed to the neglected effects of the residence time of a fluid particle in the collector.

The parameter estimates obtained with the one-node model were $0.798 \le B_1 \approx \acute{F}(\alpha\tau) \le 0.86$, 3.22 W/m^2-C $\le B_2 \approx \acute{F}U_L \le 3.89$ W/m^2-C, and 23.6 kJ/m^2-C $\le B_3 \approx C_c \le 23.8$ kJ/m^2-C. These parameter values differ by about $+6$ percent for $\acute{F}(\alpha\tau)$ and -25 percent for $\acute{F}U_L$ from the results of steady state tests given in Table 1 while this value of B_3 differs by about -3 percent from the results of transient warm-up and cool-down tests given in Table 3.

The parameters $B_{1,2,3}$ identified within the limitations of the one-node model were then used as initial estimates in the two-node model. An initial estimate of B_4 was made at this point. The gains used were unchanged from the one-node case except that $K_4 = -1$ was used, additionally. Figure 7 illustrates the greatly improved identification of parameters $B_{1,2,3}$. The parameter B_4 oscillates by about 30 percent.

The best parameter estimates produced by the two-node model were $0.794 \le B_1 \approx \acute{F}(\tau\alpha) \le 0.804$, 3.96 W/m^2-C $\le B_2 \approx \acute{F}U_L \le 4.06$ W/m^2-C, 20.3 kJ/m^2-C $\le B_3 \le 20.4$ kJ/m^2-C, and 0.173 kJ-hr/m^2-C $\le B_4 \le 0.329$ kJ-hr/m^2-C. These estimates are in reasonable agreement with the corresponding values obtained from steady-state tests. Reference to Table 1 shows only a $+2$ percent deviation in $\acute{F}(\tau\alpha)$ and a -12 percent deviation in $\acute{F}U_L$. Inspection of Fig. 3 reveals that the slope in the midrange (where the unsteady data mainly occurs) is actually somewhat smaller than the Table 1 value. Hence, the optimization result of $\acute{F}U_L \approx 4$ W/m^2-C is not as far off as its deviation from the Table 1 value suggests, and may even be the better value. Although B_3 in the two-node model cannot be directly interpreted as a heat capacitance, as explained previously, this value is about equal to the collector's effective heat capacitance given in Table 3.

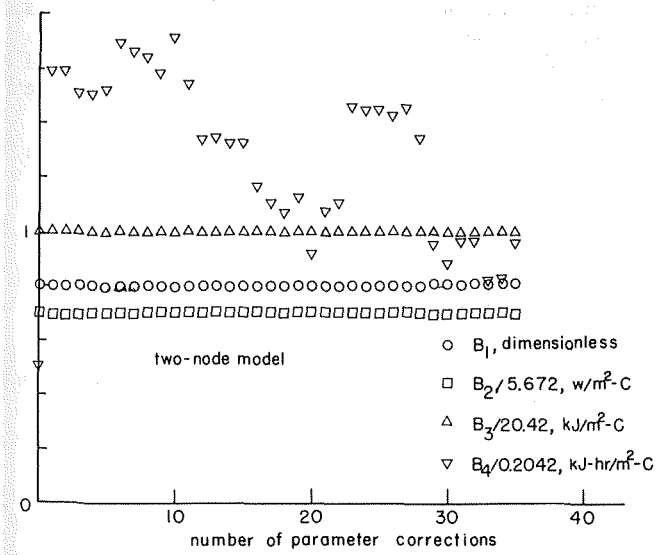

Fig. 7 Two-node model parameters versus number of parameter corrections

For convenience and easy comparison, the results of identifying the collector parameters are displayed together in Table 4.

Discussion

It has been demonstrated that the flat-plate collector parameters $\acute{F}U_L$ and $\acute{F}(\tau\alpha)$ can be identified from unsteady data. While the method employed in the present study has some deficiencies, as will be discussed, motivation for further refining work is provided by this success.

As stated earlier, in the present study parameter identification was successful only if some data were excluded from treatment as shown in Fig. 4. It is believed that this is largely due to not accurately accounting for the effect of the residence time of a fluid particle in risers and the outlet mainfold – the improved results obtained with a two-node model over those for a one-node model mainly suggest that the system is described by a partial differential equation such as describes phenomena with residence time effects. De Ron [23] and Mather [25] accounted for residence time effects in risers, but not in the outlet manifold. Hence, the needed mathematical model for predicting outlet temperature remains to be developed. Further, the best parameter identification scheme remains to be selected. It has been pointed out by others [24] that the discrete-gradient algorithm used in this study is not always the best, or even a successful, parameter identification scheme. Indeed, preliminary computational experiments suggest that the discrete-gradient algorithm of the present study cannot identify collector parameters with acceptable accuracy without excluding some data if outlet temperature measurements are in error by more than about 0.005C (0.01F). One of the algorithms successfully applied to simpler passive solar systems by Pryor, Burns, and Winn [26], Pryor and Winn [27], and Pryor et al. [28] might be considered in further refining work.

The flat-plate collector testing procedure, which a parameter identification algorithm makes possible, allows simplicity of test conditions to be traded off against simplicity of data reduction in an advantageous manner. Thus, data simply acquired under uncontrolled and realistic conditions can be utilized at the minor sacrifice of a more complex data reduction scheme. The potential advantage of such a precedure is that it is applicable to rapid testing of installed collectors in their environment of use. It is not restricted to steady conditions and could be used for on-line data reduction.

Acknowledgments

The senior author was supported by the National Aeronautics and Space Administration under Grant NSG 3087. The cooperation of the NASA-Lewis Research Center in providing test facilities is gratefully acknowledged. Computations for the discrete-gradient algorithm were performed at the University of Kansas Computation Center.

Table 4 Parameters of the NASA/Honeywell collector with $G = 48.8$ kg/hr-m^2 (10 lbm/hr-ft^2) identified by various methods

Parameter	Steady state	Transient warm-up cool-down	Discrete-gradient	
			One-node	Two-node
$\acute{F}(\tau\alpha)$, dimensionless	0.815		0.798–0.86	0.794–0.804
$\acute{F}U_L$, W/m^2-C	4.583		3.22–2.89	3.96–4.06
B_3, kJ/m^2-C		21.424–21.547	23.6–23.8	20.3–20.4
B_4, kJ-hr/m^2-C				0.173–0.329

References

1 Farber, E. A., "Solar Energy, Its Conversion and Utilization," *Solar Energy*, Vol. 14, 1973, pp. 243-252.

2 Gupta, C. L., and Garg, H. P., "Performance Studies on Solar Air Heaters," *Solar Energy*, Vol. 11, 1967, pp. 25-31.

3 McCumber, W. H., and Weston, M. W., "The Analysis and Comparison of Actual to Predicted Collector Array Performances," *IBM Journal of Research and Development*, Vol. 23, 1979, pp. 239-358.

4 Simon, F. F., and Harlamert, P., "Flat-Plate Collector Performance Evaluation—The Case for a Solar Simulation Approach," NASA TM X-71427, NASA-Lewis Research Center, Oct. 1973.

5 Simon, F. F., "Status of the NASA-Lewis Flat-Plate Collector Tests With a Solar Simulator," NASA TM X-71658, NASA-Lewis Research Center, Nov. 1974.

6 Simon, F. F., "Solar Collector Performance Evaluation With the NASA-Lewis Solar Simulator—Results for an All-Glass-Evacuated-Tubular Selectively-Coated Collector With a Diffuse Reflector," NASA TM X-71695, NASA-Lewis Research Center, Apr. 1975.

7 Simon, F. F., "Comparison Under a Simulated Sun of Two Black-Nickel-Coated Flat-Plate Solar Collectors With a Nonselective Black-Paint-Coated Collector," NASA TM X-3226, NASA-Lewis Research Center, June 1975.

8 Simon, F. F., "Flat-Plate Solar Collector Performance Evaluation With a Solar Simulator as a Basis for Collector Selection and Performance Prediction," NASA TM X-71793, NASA-Lewis Research Center, Aug. 1975.

9 Simon, F. F., "An Experimental Investigation With Artificial Sunlight of a Solar Hot Water Heater," NASA TM X-73534, NASA-Lewis Research Center, Aug. 1976.

10 Hottel, H. C., "Performance of Flat-Plate Solar Energy Collectors," *Proceedings of the Symposium on Space Heating with Solar Energy*, M.I.T., 1959, pp. 58-71.

11 Bliss, R. W., Jr., "The Derivations of Several Plate-Efficiency Factors Useful in the Design of Flat-Plate Solar Heat Collectors," *Solar Energy*, Vol. 3, 1959, pp. 55-64.

12 Klein, S. A., Duffie, J. A., Beckman, W. A., "Transient Considerations of Flat-Plate Solar Collectors," *Journal of Engineering for Power*, Vol. 96, 1974, pp. 109-113.

13 Whillier, A., "Solar Energy Collection and Its Utilization for House Heating," Sc. D. Thesis, Department of Mechanical Engineering, M.I.T., 1953.

14 Duffie, J. A., and Beckman, W. A., *Solar Energy Thermal Processes*, John Wiley & Sons, New York, 1974.

15 Close, D. J., "A Design Approach for Solar Processes," *Solar Energy*, Vol. 11, 1967, pp. 112-122.

16 "Method of Testing to Determine the Thermal Performance of Solar Collectors," ASHRAE Standard 93-77, ASHRAE, New York, 1977.

17 Hotchkiss, G. B., "Comparison of Three Experimental Methods Used in Determining the Thermal Performance of Flat-Plate Solar Collectors," Doctor of Engineering Report, Mechanical Engineering Department, University of Kansas, 1978 (see also NASA TM X-78929, NASA-Lewis Research Center, Oct. 1978 of the same title and author).

18 Simon, F. F., and Buyco, E. H., "Outdoor Flat-Plate Collector Performance Prediction from Solar Simulator Test Data," NASA TM X-71707, NASA-Lewis Research Center, May 1975.

19 Sehitoglu, H., and Klein, R. E., "A Finite Element and Gradient Method for Identification of Parameters in a Class of Distributed Parameter Systems," ASME Paper 78-WA/DSC-29.

20 Bekey, G. A., and Karplus, W. J., *Hybrid Computation*, John Wiley & Sons, New York 1968, pp. 244-300.

21 Stofer, C. E., "A Discrete Gradient Optimization Algorithm for the On-Line Determination of Parameters of Process Models," Ph.D. Thesis, Chemical and Petroleum Engineering Department, University of Kansas, 1970.

22 Drake, N. H., "A Computer Study of a Discrete Gradient Optimization Method as Applied to Topologically Exact Models," Master of Science Thesis, Chemical and Petroleum Engineering Department, University of Kansas, 1969.

23 De Ron, A. J., "Dynamic Modeling and Verification of A Flat-Plate Solar Collector," *Solar Energy*, Vol. 24, 1980, pp. 117-128.

24 Lau, W. K. J., "An Algorithm For The Estimation of Parameters in Models Defined by Differential Equations Based on Sensitivity Analyses," Master of Science Thesis, Chemical and Petroleum Engineering Department, University of Kansas, 1981.

25 Mather, G. R., "Transient Response of Solar Collectors" ASME JOURNAL OF SOLAR ENERGY ENGINEERING, Vol. 104, 1982, pp. 165-172.

26 Pryor, D. V., Burns, P. J., and Winn, C. B., "Parameter Estimation In Passive Solar Structures," *Proc. 5th Ann. Passive Solar Conf.*, Amherst, Mass., Oct. 1980.

27 Pryor, D. V., and Winn, C. B., "A Sequential Filter Used for Parameter Estimation in a Passive Solar System," *Solar Energy*, Vol. 28, 1982, pp. 65-73.

28 Pryor, D. V., et al., "Parameter Estimation in Solar Systems by the Method of Least Squares," *Proc. JACC*, San Francisco, Calif. Aug. 1980.

APPENDIX

Discrete-Gradient Optimization Algorithm An objective function f is chosen so that it is an algebraic function of the vector of mathematical model parameters $\bar{B}$ so that $f=f(\bar{B})$ where $\bar{B}=[B_1, B_2, \ldots, B_n]^T$. If there are n unknown parameters in the mathematical model, the differential change in the objective function caused by differential changes of the parameters is given by

$$df = (\partial f/\partial B_1)dB_1 + (\partial f/\partial B_2)dB_2 + \ldots + (\partial f/\partial B_n)dB_n$$

or,

$$df = \nabla f^T \cdot d\bar{B}$$

where

$$\nabla f^T = [\partial f/\partial B_1, \partial f/\partial B_2, \ldots, \partial f/\partial B_n]$$

and

$$d\bar{B} = [dB_1, dB_2, \ldots, dB_n]^T$$

To change the objective function quickly, it is desirable to make df large. The dot product of two vectors reaches its maximum value when the two vectors are parallel or, in other words, when corresponding components of the two vectors are proportional to one another as

$$d\bar{B} = K \nabla f$$

where K is a constant. A positive K causes f to increase while a negative K causes f to decrease.

The objective function is defined now to be

$$f = \int_{t_i}^{t_i+\Delta t} (e^2/2)dt \qquad (A\text{-}1)$$

where e is the instantaneous difference between the predicted output of a mathematical model and the measured output of a physical process. Also, Δt is a fixed time interval of the integration. The objective function is the integral of the squares of the instantaneous errors over Δt. The mathematical model's parameters are constant for $t_i < t \le t_i + \Delta t$ so that f is a function of the parameters, allowing ∇f to be evaluated. The objective function defined by equation (A-1) leads to a discrete, rather than a continuous, optimization procedure as Bekey and Karplus [20] observed. Thus, the differential change in the parameter vector $d\bar{B}$ must be replaced by the discrete change $\Delta\bar{B}$. Hence,

$$\Delta\bar{B} = K \nabla f \qquad (A\text{-}2)$$

Consider next a mathematical model which is

$$d^2y/dt^2 + (B_3/B_4)dy/dt = [2B_1 I - B_2(y + T_i - 2T_a) - 2G\, C_p(y - T_i)]/B_4 \qquad (A\text{-}3)$$

subject to the initial conditions

$$dy(t_i)dt = dT_0(t_i)/dt, \quad y(t_i) = T_i(t_i)$$

where t_i, T_a, and GC_p are known constants. Here, $y(t)$ is the output of the mathematical model whose known input is $I(t)$ while $T_0(t)$ is the measured output of the physical process with the same inputs. The objective function then is

$$f = \int_{t_i}^{t_i+\Delta t} [(y - T_0)^2/2]dt$$

since $e = y - T_0$. Noting that T_0 does not depend on the mathematical model's parameters, the derivative of f with respect to a model parameter B_n is

$$\partial f/\partial B_n = \int_{t_i}^{t_i+\Delta t} e\, u_n\, dt \qquad (A\text{-}4)$$

with $u_n = \partial y/\partial B_n$ being a sensitivity coefficient and $n = 1,2,3,4$.

The sensitivity coefficient $u_n = \partial y/\partial B_n$ can be obtained by differentiating equation (A-3) with respect to B_n to obtain a differential equation for u_n. Taking $n = 1$, for example, this procedure gives

$$\partial(d^2y/dt^2)/\partial B_1 + (B_3/B_4)\partial(dy/dt)/\partial B_1 = [2I - (B_2 + 2GC_p)\partial y/\partial B_1]/B_4$$

subject to the initial conditions (since $T_0(t_i)$ does not depend on B_1) of

$$\partial(\partial y(t_i)/\partial t)\partial B_1 = 0, \quad \partial y(t_i)/\partial B_1 = 0$$

Interchanging the order of differentiation and recalling that $u_1 = \partial f/\partial B_1$ gives

$$d^2u_1/dt^2 + (B_3/B_4)du_1/dt = [2I - (B_2 + 2G\ C_p)u_1]/B_4 \tag{A-5a}$$

with $du_1(t_i)/dt = 0$, $u_1(t_i) = 0$. Proceeding in a similar fashion for $n = 2, 3, 4$, yields

$$d^2u_2/dt^2 + (B_3/B_4)du_2/dt = -[y + T_i - -2T_a + (B_2 + 2G\ C_p)u_2]/B_4 \tag{A-5b}$$

$$du_2(t_i)/dt = 0, \quad u_2(t_i) = 0$$

$$d^2u_3/dt^2 + (B_3/B_4)du_3/dt = -[dy/dt + (B_2 + 2G\ C_p)u_3]/B_4 \tag{A-5c}$$

$$du_3(t_i)/dt = 0, \quad u_3(t_i) = 0$$

$$d^2u_4/dt^2 + (B_3/B_4)du_4/dt = [(B_3/B_4)dy/dt - \{2B_1I - B_2(y + T_i - 2T_a) - 2G\ C_p(y - T_i)\}/B_4 - (B_2 + 2G\ C_p)u_4]/B_4 \tag{A-5d}$$

$$du_4(t_i)/dt = 0, \quad u_4(t_i) = 0$$

An adaptive modeling procedure proceeds as follows. Initial estimates are made for the model's parameters (B_1, B_2, B_3, B_4). The process output T_0 is measured continuously and is compared with the model's predicted output y to generate an error $e = y - T_0$ which is integrated for a time interval Δt. During this interval the various influence coefficients u_n are computed according to equation (A-5) which requires use of the model's output y and first derivative dy/dt. During this time interval, changes in the model's parameters are computed as specified by equations (A-2) and (A-4) so that

$$\Delta B_1 = K_1 \int_{t_i}^{t_i + \Delta t} e\ u_1\ dt \tag{A-6a}$$

$$\Delta B_2 = K_2 \int_{t_i}^{t_i + \Delta t} e\ u_2\ dt \tag{A-6b}$$

$$\Delta B_3 = K_3 \int_{t_i}^{t_i + \Delta t} e\ u_3\ dt \tag{A-6c}$$

$$\Delta B_4 = K_4 \int_{t_i}^{t_i + \Delta t} e\ u_4\ dt \tag{A-6d}$$

Note that the values of K_n are not required to be equal. After the interval Δt has elapsed the model, equation (A-3), is reset to the current values of the process' output and first derivative. The model parameters are then incremented by the amounts calculated by equation (A-6) and the procedure, constituting a discrete-gradient optimization algorithm, is repeated.

After a number of iterations the objective function f has been reduced to a minimum value and the parameters of the process have been identified.

If the mathematical model is taken to be

$$dy/dt = [2B_1I - B_2(y + T_i - 2T_a) - 2G\ C_p(y - T_i)]/B_3 \tag{A-7}$$

subject to the initial condition of $y(t_i) = T_0(t_i)$, a similar treatment leads to a similar result. The sensitivity coefficients are obtained from

$$du_1/dt = [2I - (B_2 + 2G\ C_p)u_1]/B_3 \tag{A-8a}$$

$$u_1(t_i) = 0$$

$$du_2/dt = [y + T_i - 2T_a + (B_2 + 2G\ C_p)u_2]/B_3 \tag{A-8b}$$

$$u_2(t_i) = 0$$

$$du_3/dt = -[dy/dt + (B_2 + 2G\ C_p)u_3]/B_3 \tag{A-8c}$$

$$u_3(t_i) = 0$$

and the changes in parameter values are obtained from equations (A-6a)-(A-6c).

Additional examples of the application of the discrete-gradient optimization method are given by Stofer [21] and by Drake [22].